Gold Nanoparticles

DOI: 10.1002/anie.201204699

Protein-Assisted One-Pot Synthesis and Biofunctionalization of Spherical Gold Nanoparticles for Selective Targeting of Cancer Cells**

Miriam Colombo, Serena Mazzucchelli, Veronica Collico, Svetlana Avvakumova, Laura Pandolfi, Fabio Corsi, Francesca Porta, and Davide Prosperi**

Gold nanoparticles (AuNPs) are stimulating increasing interest because of their unique size-dependent electronic and optical properties combined with their great potential in biomedicine as sensors, diagnostic agents, heating mediators for cancer thermotherapy, and drug delivery vehicles.[1–4] However, for nanoparticles to become suitable for use in biology, they require appropriate modification with biomolecules, which confer a specific function to the nanoconjugate.[5] Proteins are particularly advantageous as they can impart both colloidal stability and bioactivity to nanoparticles.[6–9] There are two main approaches to introduce stably bound proteins onto the AuNP surface. Most strategies involve the fabrication of monodisperse AuNPs followed by post-synthetic conjugation.[10–12] Unfortunately, it is extremely difficult to achieve a controlled arrangement of protein molecules on the gold surface in this way and this arrangement may affect the biofunctionality of the nanoconjugate.[13] The arrangement of the molecules is particularly relevant for proteins with specific targeting activity, such as monoclonal antibodies, for which we showed that the conservation of structural features may depend on the choice of the immobilization route.[14] More recently, an alternative approach has been proposed that exploits the characteristics of some proteins to behave as templates for AuNP formation in an aqueous environment.[15,16] Most examples used bovine serum albumin (BSA);[17] however, BSA has limited biological activity and was demonstrated to be partially unfolded upon gold incorporation.[18] Because of the high affinity of sulfur for gold, cysteines have been postulated to be the preferred conjugation sites on the protein for gold seeding and for AuNP complexation.[16]

Although the mechanism of protein assistance in nanoparticle formation is still poorly understood,[19] we explored the possibility to generate gold nanoconjugates in aqueous solution by using a protein as a colloidal stabilizer, by employing a synthetic approach set up recently with peptide/AuNPs (peptide = $(GC)_2$ and $RDG(GC)_2$).[20] In that case, the molecular targeting capability of the immobilized peptide could be preserved. We have recently reported on a non-immunogenic engineered B-domain variant of protein A (spaBC3, 7.5 kDa) suitable for site-specific conjugation of antibodies (for example, Imumoglobulin G; IgG).[21] Interestingly, 1) the protein structure was preserved over a broad range of pH (pH 2–12), 2) the IgG–spaBC3 complex dissociated only below pH 4.5 (e.g., in lysosomes), and 3) it could bind human IgG antibodies with high affinity toward their Fc fragment through the consensus sequence consisting of Gln184-Gln185-Asn186-Phe188-Tyr189-Leu192-Asn203-Ile206-Glu207-Lys210 (Figure 1).

In this work, we present a new method for the development of stable, spherical AuNPs; this method involves the use of spaBC3 as a capping agent in the colloidal reduction of a gold salt precursor, thus resulting in a controlled surface functionalization of the gold particle suitable for binding with human IgGs. SpaBC3-functionalized AuNPs (PANPs) present several important advantages for biological application: 1) the synthetic parameters can be optimized to generate highly uniform colloidal dispersions with finely tunable size, 2) the resulting bio-nanoparticles are stable in a physiological

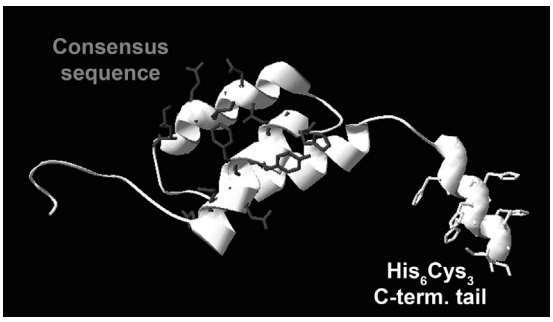

Figure 1. 3D model of spaBC3 obtained by modifying a 1SS1 pdb file with pdb viewer. The immunoglobulin G (IgG) binding consensus sequence is highlighted in gray, and the His_6Cys_3 C-terminal tail is reported in white.

[*] Dr. M. Colombo,[+] Dr. D. Prosperi
NanoBioLab, Dipartimento di Biotecnologie e Bioscienze
Università degli Studi di Milano-Bicocca
Piazza della Scienza 2, 20126 Milano (Italy)
and
Fondazione Don Carlo Gnocchi Onlus
via Capecelatro 66, 20148 Milano (Italy)
E-mail: davide.prosperi@unimib.it

Dr. M. Colombo,[+] Dr. S. Mazzucchelli,[+] L. Pandolfi, Prof. F. Corsi
Dipartimento di Scienze Biomediche e Cliniche "Luigi Sacco"
Università degli Studi di Milano
via G. B. Grassi 74, 20157 Milano (Italy)

V. Collico, S. Avvakumova, Prof. F. Porta
Dipartimento di Chimica, Università degli Studi di Milano
via C. Golgi 19, 20133 Milano (Italy)
E-mail: francesca.porta@unimi.it

[+] These authors contributed equally to this work.

[**] M.C., S.M., and L.P. acknowledge the research fellowships of CMENA. We thank R. Allevi for TEM images and Fondazione Filarete for G-STED. This work was supported by NanoMeDia Project (Regione Lombardia), "Fondazione Romeo e Enrica Invernizzi" and Fondazione CARIPLO 2009-2696.

Supporting information for this article is available on the WWW under http://dx.doi.org/10.1002/anie.201204699.

environment for months, and 3) spaBC3 works as a bifunctional biolinker, acting concomitantly as a stabilizer for AuNP nucleation and growth steps, and as a bioactive functionality that is ideal for the efficient immobilization of human IgGs on AuNPs with an optimal presentation of their target-directed Fab fragments.

As spaBC3 presents a His_6Cys_3 C-terminal sequence connected to the Fc-binding domain by a loop (Figure 1), we speculated that both the Cys thiols and the polyHis could interact with $AuCl_4^-$ ions, to trigger the nucleation and growth of AuNPs upon addition of $NaBH_4$ at pH 3.6–3.8. The synthetic procedure illustrated in Scheme 1 was simple and compatible with protein requirements, yielding a very stable,

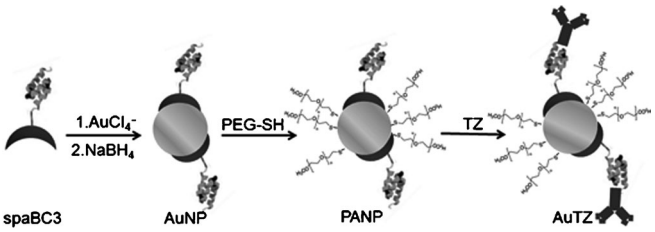

Scheme 1. Synthesis of PANP and AuTZ.

red sol of PANPs. Excess proteins and ions were removed by centricon filtration (30 kDa cutoff), and then the Au–spaBC3 nanoparticles were washed several times with water and reduced to a final concentration of 3.8 nM. The concentration value was obtained from the measured absorbance at 517 nm on the basis of a specific calibration curve (see the Supporting Information).

The dimension and morphology of PANPs were tuned by varying the Au/spaBC3 molar ratio (representative examples are shown in Table 1). The various sols showed resonance plasmon peaks in the 514–520 nm region of the UV/Vis

Table 1: PANP properties in relation to the Au/spaBC3 ratio.

Molar ratio spaBC3[$\times10^{-4}$]/$AuCl_4^-$	Plasmon band λ_{max}/nm	Mean diameter[a] d/nm
2.5:1	517	6.2 ± 1.2
7:1	522	5.3 ± 1.4
8:1	519	5.1 ± 1.0
9:1	520	4.8 ± 1.4

[a] Size was determined by 300 counts in each TEM image.

spectra. The optimal spaBC3/$AuCl_4^-$ ratio was 2.5×10^{-4}:1 (Figure 2), the use of which resulted in spherical AuNPs ($d=6.2\pm1.2$ nm) coated by an average of 2–4 molecules per PANP, as determined by a Bradford assay. When we used this molar ratio all spaBC3 molecules were believed to be involved in AuNP capping, because, within the limits of UV sensitivity, no trace protein was detected in either the supernatant or the washings. The presence of spaBC3 bound to AuNPs was assessed by using FTIR and observing the disappearance, in the PANP spectrum, of the weak band, at 2579 cm^{-1}, attributed to the S–H stretching mode in spaBC3 Cys (see the Supporting Information). The theoretical surface

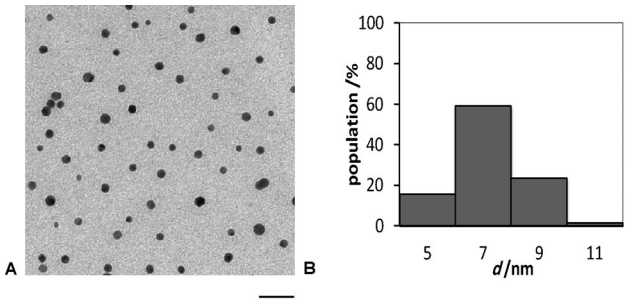

Figure 2. TEM micrographs and size distribution histogram of PANPs from spaBC3/$AuCl^{4-}$ molar ratio of 2.5×10^{-4}:1. Scale bar = 50 nm.

area of the binding region of spaBC3 is 13.0×16.4 Å, as determined by a 3D protein model, but the overall apparent volume of spaBC3 is much larger ($59.8\times22.0\times20.7$ Å). This result implies that uncoated surface is still available after PANP isolation, thus leading to nonspecific adsorption of undesired material in a biological milieu. Moreover, when PANPs were suspended in a high-ionic-strength solution, such as a phosphate buffer saline, pH 7.4 (PBS), a tendency to aggregate was detected, as observed by a red-shifted Au^0 plasmon band in UV/Vis spectra and the violet color of the sols. Thus, PANPs were treated with PEG–SH (MW 2 kDa). Pegylated PANPs showed unchanged absorbance and wavelength of the plasmonic band even at 6 M NaCl concentration. The presence of both bound spaBC3 and PEG chains in pegylated PANPs was confirmed by FTIR, in which protein amide I and II bands (1642 and 1558 cm^{-1}, respectively) and a band corresponding to $\nu_{C\text{-}O\text{-}C}$ of PEG chain (1086 cm^{-1}), were both present and even slightly shifted from free spaBC3 and PEG–SH values. As expected, the hydrodynamic size of PANPs was slightly changed from 46.9 ± 1.4 nm to 48.8 ± 1.1 nm upon pegylation, whereas the ζ potential was reduced from -27.5 ± 2.1 mV to -19.9 ± 5.1 mV. The colloidal stability of pegylated PANPs was also demonstrated between pH 2 and 11 (see the Supporting Information); this stability is probably due to the good protein stability in that pH range.[21]

To demonstrate the utility of PANPs as an ideal nanoplatform for the efficient and oriented conjugation of IgGs, we assessed the extent of preserved bioactivity of spaBC3 in PANPs. As a proof of principle, we used trastuzumab (TZ), a humanized monoclonal antibody known in clinical practice for the treatment of breast carcinoma because of its high affinity for HER2-positive ($HER2^+$) breast cancer cells.[22,23] Pegylated PANPs were incubated in PBS with purified TZ for 1 hour at 25 °C. After incubation, TZ-functionalized PANPs (AuTZ) were dialyzed through a 1000 kDa cutoff membrane to remove the unreacted TZ. Purified AuTZ were stable in PBS and were characterized by dynamic light scattering (DLS; 66.8 ± 2.3 nm), ζ potential (-13.5 ± 4.2 mV), FTIR, and UV/Vis measurements, which suggested the presence of two TZ per AuTZ. Moreover, the strength of interaction between PANP and TZ was assessed by washing AuTZ in citrate buffer at pH 3.0, a process which was expected to remove TZ from PANP surface. Dot-blot results, however, demonstrated that after 1 hour of incubation, TZ was still present on nanoparticles (see the Supporting Information).

The selectivity of TZ binding by specific interaction with spaBC3 was assessed by dot blot of PANPs before and after TZ incubation (Figure 3). Results showed that PANPs specifically recognized TZ, in comparison with fully pegylated citrate–AuNPs (CNPs), which were used as a negative control. Moreover, the similarity of the chemiluminescence signal observed in PANPs after TZ incubation, and in TZ alone,

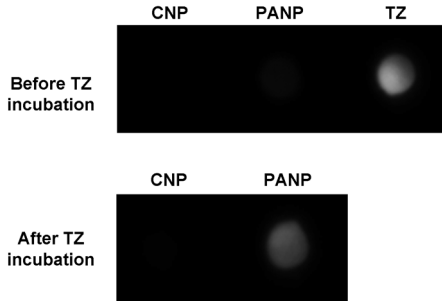

Figure 3. Dot-blot assay of PANPs before and after TZ immobilization. PANPs (1 μg) and pegylated citrate-AuNPs (CNPs, 1 μg) were filtered through a polyvinylidene difluoride membrane before and after TZ conjugation, then probed with anti-human-HRP antibody, and revealed with an enhanced chemioluminescence (ECL) substrate. An equal amount of TZ loaded onto PANPs was used as positive control.

used as a positive control, corroborated our calculation of the presence of about two TZ per nanoparticle. The generality of the method was also assessed with other antibodies (see the Supporting Information).

Next, we moved to the evaluation of the AuTZ targeting efficiency toward HER2$^+$ MCF7 cells. AuTZ were incubated with MCF7 cells (5×10^5 cells) for 1 hour at two different concentrations, 5 μg mL^{-1} and 50 μg mL^{-1} (see the Supporting Information). Cells were washed and subjected to FACScan analysis. Flow cytometry was performed with an anti-human secondary antibody labeled with Alexa Fluor 488. Results showed a substantial right-shift of fluorescence signal even at the lowest concentration; this shift is consistent with a good labeling efficiency of AuTZ toward HER2$^+$ cells. As a positive control, MCF7 cells were also incubated with free TZ at concentrations corresponding to those contained in the above AuTZ (0.9 and 9.0 μg mL^{-1} TZ), and these results confirmed the same trend observed with AuTZ and supported our previous quantification of the number of TZ molecules immobilized on PANPs. In contrast, when AuTZ were incubated with HER2-negative (HER2$^-$) MDA cells, no fluorescence labeling was observed even at the highest concentration, thus suggesting that cell labeling was specific for HER2$^+$ cells.

The interaction of AuTZ with cells was assessed by confocal laser scanning microscopy on MCF7 and MDA cells treated with 50 μg mL^{-1} AuTZ and a corresponding amount of free TZ (Figure 4). No fluorescence signal was observed with MDA cells incubated up to 1 hour, whereas MCF7 cells were labeled by AuTZ already after 15 minutes both at the membrane and inside the cell. Free TZ was recovered only at the HER2$^+$ cell membrane at this stage, presumably in correspondence to HER2 receptor sites. However, after

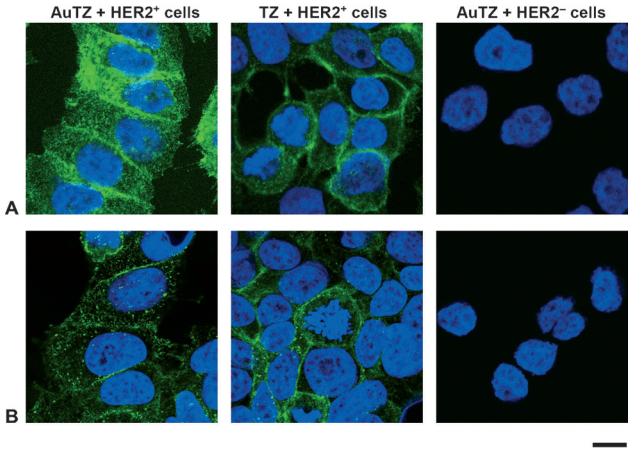

Figure 4. HER2$^+$ cells (MCF7) were incubated for 15 min (A) or 1 h (B) at 37 °C with AuTZ (50 μg mL^{-1}). TZ (0.9 μg mL^{-1}) incubated on MCF7 was used as positive control, while AuTZ (50 μg mL^{-1}) incubated with HER2$^-$ cells (MDA) was used as negative control. TZ was revealed by an Alexa Fluor 488-labeled secondary antibody (green). Nuclei were stained with DAPI (blue). Scale bar = 10 μm.

1 hour, AuTZ had completed their penetration process and were observed only inside the cell, whereas free TZ was still mostly localized on the outer membrane. This result suggested a marked increase in cell penetration assisted by nanoparticles, as we have observed previously in vivo.[24] CW-STED confocal images corroborated the confocal images and allowed us to discriminate single nanoparticles inside cells to confirm that the AuTZ were not aggregated even inside the cellular compartments (Figure 5).

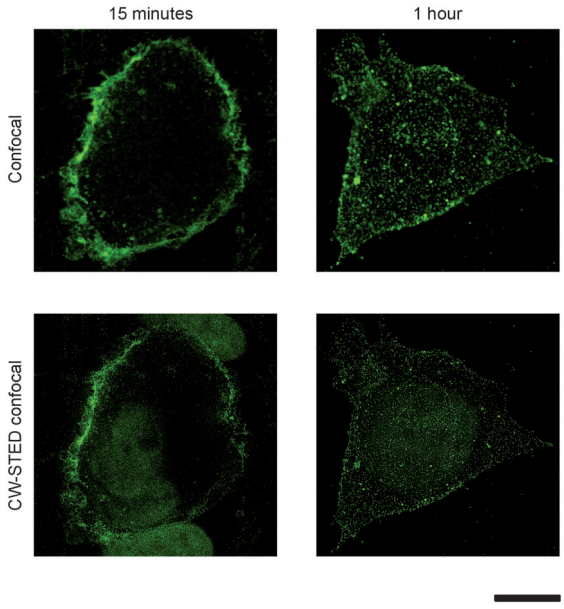

Figure 5. Comparison between confocal and CW-STED (continuous-wave stimulated emission depletion) confocal images of HER2$^+$ cells (MCF7) incubated for 15 min or 1 h at 37 °C with AuTZ (50 μg mL^{-1}). TZ was revealed by an Alexa Fluor 488-labeled secondary antibody (green). Scale bar = 10 μm.

Finally, cell proliferation and death from AuTZ were investigated (see the Supporting Information). Interestingly, we did not observe any sedimentation of nanoparticles even after 72 hours, thus further corroborating our data on the remarkable stability of AuTZ in physiological media. No differences were observed between untreated and AuTZ-treated cells in terms of viability at 50 $\mu g\,mL^{-1}$ after 72 hours. AuTZ were also found to be nontoxic at 5 and 50 $\mu g\,mL^{-1}$ in MCF7 after 24 hours of exposure. These experiments suggested an excellent safety of AuTZ in cell cultures.

In summary, we have reported an innovative one-step synthesis and biofunctionalization of AuNPs using a small variant of protein A as a biotemplate. This biotemplate behaves as a thiolate ligand capable of interacting with the AuNP surface and controlling the nanoparticle nucleation and growth, thus allowing the nanoparticle size to be finely tuned. A first clear advantage of this approach was that it allowed us to obtain high-quality AuNPs in the water phase, and therefore avoid the transfer from organic solvents, which usually results in a lack of long-term stability. Second, spaBC3 maintained its original capability of binding IgGs with high affinity by their Fc region, thus providing a highly efficient bio-nanoparticle system suitable for selective cell labeling by membrane-receptor-specific recognition. In view of the tremendous utility of monoclonal antibodies in cell research as well as in diagnosis and therapy of malignancies, and of their excellent colloidal stability in buffers and media, we envision that our PANPs may become attractive as a simple universal method for antibody nanolabeling virtually applicable to every human IgG.

Received: June 15, 2012
Published online: July 25, 2012

Keywords: antibodies · gold · nanoparticles · protein template · tumor targeting

[1] E. C. Dreaden, A. M. Alkilany, X. Huang, C. J. Murphy, M. A. El-Sayed, *Chem. Soc. Rev.* **2012**, *41*, 2740 – 2779.
[2] R. A. Sperling, P. R. Gil, F. Zhang, M. Zanella, W. J. Parak, *Chem. Soc. Rev.* **2008**, *37*, 1896 – 1906.
[3] C. Kim, S. S. Agasti, Z. Zhu, L. Isaacs, V. M. Rotello, *Nat. Chem.* **2010**, *2*, 962 – 966.
[4] L. Vigderman, P. Manna, E. R. Zubarev, *Angew. Chem.* **2012**, *124*, 660 – 665; *Angew. Chem. Int. Ed.* **2012**, *51*, 636 – 641.
[5] D. A. Giljohann, D. S. Seferos, W. L. Daniel, M. D. Massich, P. C. Patel, C. A. Mirkin, *Angew. Chem.* **2010**, *122*, 3352 – 3366; *Angew. Chem. Int. Ed.* **2010**, *49*, 3280 – 3294.
[6] M. Colombo, S. Sommaruga, S. Mazzucchelli, L. Polito, P. Verderio, P. Galeffi, F. Corsi, P. Tortora, D. Prosperi, *Angew. Chem.* **2012**, *124*, 511 – 514; *Angew. Chem. Int. Ed.* **2012**, *51*, 496 – 499.
[7] R. Lévy, N. T. K. Thanh, R. C. Doty, I. Hussain, R. J. Nichols, D. J. Schiffrin, M. Brust, D. G. Fernig, *J. Am. Chem. Soc.* **2004**, *126*, 10076 – 10084.
[8] A. Schroedter, H. Weller, *Angew. Chem.* **2002**, *114*, 3346 – 3350; *Angew. Chem. Int. Ed.* **2002**, *41*, 3218 – 3221.
[9] M. Colombo, S. Mazzucchelli, J. M. Montenegro, E. Galbiati, F. Corsi, W. J. Parak, D. Prosperi, *Small* **2012**, *8*, 1492 – 1497.
[10] W. R. Algar, D. E. Prasuhn, M. H. Stewart, T. L. Jennings, J. B. Blanco-Canosa, P. E. Dawson, I. L. Medintz, *Bioconjugate Chem.* **2011**, *22*, 825 – 858.
[11] N. Erathodiyil, J. Y. Ying, *Acc. Chem. Res.* **2011**, *44*, 925 – 935.
[12] J. M. Abad, S. F. L. Mertens, M. Pita, V. M. Fernandez, D. J. Schiffrin, *J. Am. Chem. Soc.* **2005**, *127*, 5689 – 5694.
[13] I. Medintz, *Nat. Mater.* **2006**, *5*, 842.
[14] E. Occhipinti, P. Verderio, A. Natalello, E. Galbiati, M. Colombo, S. Mazzucchelli, P. Tortora, S. M. Doglia, D. Prosperi, *Nanoscale* **2011**, *3*, 387 – 390.
[15] M. B. Dickerson, K. H. Sandhage, R. R. Naik, *Chem. Rev.* **2008**, *108*, 4935 – 4978.
[16] D. L. Feldheim, B. E. Eaton, *ACS Nano* **2007**, *1*, 154 – 159.
[17] J. L. Burt, C. Gutiérrez-Wing, M. Miki-Yoshida, M. José-Yacaman, *Langmuir* **2004**, *20*, 11778 – 11783.
[18] P. Khullar, V. Singh, A. Mahal, P. N. Dave, S. Thakur, G. Kaur, J. Singh, S. S. Kamboj, M. S. Bakshi, *J. Phys. Chem. C* **2012**, *116*, 8834 – 8843.
[19] H. Wei, Z. Wang, J. Zhang, S. House, Y.-G. Gao, L. Yang, H. Robinson, L. H. Tan, H. Xing, C. Hou, I. M. Robertson, J.-M. Zuo, Y. Lu, *Nat. Nanotechnol.* **2011**, *6*, 93 – 97.
[20] G. Scarì, F. Porta, U. Fascio, S. Avvakumova, V. Dal Santo, M. De Simone, M. Saviano, M. Leone, A. Del Gatto, C. Pedone, L. Zaccaro, *Bioconjugate Chem.* **2012**, *23*, 340 – 349.
[21] S. Mazzucchelli, M. Colombo, C. De Palma, P. Verderio, M. D. Coghi, E. Clementi, P. Tortora, F. Corsi, D. Prosperi, *ACS Nano* **2010**, *4*, 5693 – 5702.
[22] A. Clifford, M. D. Hudis, *N. Engl. J. Med.* **2007**, *357*, 39 – 51.
[23] M. Colombo, F. Corsi, D. Foschi, E. Mazzantini, S. Mazzucchelli, C. Morasso, E. Occhipinti, L. Polito, D. Prosperi, S. Ronchi, P. Verderio, *Pharmacol. Res.* **2010**, *62*, 150 – 165.
[24] F. Corsi, L. Fiandra, C. De Palma, M. Colombo, S. Mazzucchelli, P. Verderio, R. Allevi, A. Tosoni, M. Nebuloni, E. Clementi, D. Prosperi, *ACS Nano* **2011**, *5*, 6383 – 6393.

